www.amlett.org, www.amlett.com, DOI:10.5185/amlett.2013.icnano.283
"ICNANO 2011" Special Issue Published online by the VBRI press in 2013

Effect of alumina reinforcing fillers in BisGMA-based resin composites for dental applications

Sanjay Thorat[1,2], Alberto Diaspro[2], Marco Salerno[2,*]

[1]*University of Genova, viale Causa 13, I-16145 Genova, Italy*
[2]*Istituto Italiano di Tecnologia, Nanophysics Department, via Morego 30, I-16163 Genova, Italy*

*Corresponding author. Tel: (+39) 10-71 781444; Fax: (+39) 10-720321; E-mail: marco.salerno@iit.it

ABSTRACT

A photo-polymerizable resin based on bisphenol-A-glycidyldimethacrylate monomer was loaded at both 10 and 50% by weight with particles of alumina of size scales in the 10 micrometers and submicrometer order, termed micro-alumina and nano-alumina, respectively. After curing, the viscoelastic properties of these materials were characterized by multifrequency dynamic mechanical analysis at 0.1, 1 and 10 Hz, carried out in bending mode under strain control across the range of temperatures of 2 to 62°C, normally occurring in the mouth. The storage moduli close to body temperature (37°C) and mastication frequency (1 Hz) was evaluated as the main result of the analysis, along with its change on frequency. The stiffest composite was the 50%wt loaded nano-alumina, which reached a modulus of ~6.8 GPa, comparable to those of commercial restorative composites, even in the absence of bonding agent coating of the fillers. The storage moduli at the same frequency but room temperature (25°C) were compared with the elastic modulus resulting from atomic force microscopy nanoindentation. These measurements confirmed the same ranking of materials as the dynamic flexural analysis, while providing elastic modulus values ~50% higher on average. From the dynamic analysis no thermal transition was observed in the considered temperature range, and a stiffening effect appeared at higher frequencies for all the composites. Copyright © 2013 VBRI press.

Keywords: Dental restorative composites; inorganic fillers; dynamic mechanical analysis; nanoindentation; elastic modulus.

Sanjay Balkrishna Thorat received his MSc in Industrial Chemistry from Shivaji University (Kolhapur, India) in 2005. He worked on catalysis in Pune, first for the Indian National Chemical Laboratory (2005-2007), then for the Dow Chemical R&D center (2007-2009). In 2010 he was Research Assistant at the Korea Institute of Energy Research. In January 2011 he joined the Italian Institute of Technology (IIT) of Genoa as a PhD student. His main topic is the development of innovative dental restorative composites. Since the beginning of his PhD he has published four research papers on international refereed journals

Alberto Diaspro received is doctoral degree in electronic engineering in 1983 in Genoa, where he founded the Laboratory for Advanced Microscopy, Bioimaging and Spectroscopy, and became Head of the IIT Nanophysics Unit. He is President of Optics With Life Sciences, former President of European Biophysical Societies Association, and active member of SPIE and Italian Physical Society. He was visiting scientist at Drexel University, Universidad Autonoma de Madrid, Czech Academy of Sciences, Polytechnic University of Bucharest, University of Illinois at Urbana- Champaign. He has been invited speaker at more than 200 international conferences, and is author of more than 170 international publications.

Marco Salerno received his MSc in Physics in Pisa in 1993, on FFM. In 1995-1998 he worked on AFM at the Scientific-Technological Park of Elba Island (Leghorn). He received his PhD for SNOM of gold nanoparticle Plasmons in Graz (Austria) in 2002. In 2003 he was a postdoc in EC-STM of metalloproteins in Modena. In 2004-2006 he worked in clean room fabrication of polymer DFB lasers, at the National Nanotechnology Lab in Lecce. In 2007 he joined IIT Genova where he founded the SPM Lab. His research interests are in dental materials and anodic porous alumina. He is co-author of more than 50 international papers

Introduction

The use of composites as dental restoratives is steadily increasing since several decades [**1-3**]. Novel opportunities appeared recently with the application of nanotechnology, especially regarding the potential use of newly available nano-particle forms of several materials [**4, 5**]. Additionally, the long standing competitor amalgam, though still better performing from the mechanical point of view [**6**], is today about to be banned completely both for aesthetical reasons and the potential mercury hazards, as also recently recommended in a European directive [**7**]. Therefore, continuous research in this field is undergoing, and particularly for the mechanical properties a detailed

investigation of materials in the laboratory is recommended before moving on to the clinical applications, for their appropriate interpretation [**8-11**].

In this work we investigated simple composite systems without filler-matrix bonding agent, and within this limitation we studied the effect of two different classes of particles size for the same filler material. For the latter, in the quest for stiffer composites for posterior applications, our choice fell on alumina. This material has already been investigated as a filler in bone cements [**12, 13**], but its use as dental restorative composite is relatively new [**14**]. The alumina composites have been compared to both bare resin, termed negative control (working as a lower limit for the elastic modulus of the composites), and glass composites with the same loading, termed positive controls (as opposite to the low modulus bare resin).

Whereas until one decade ago the most used techniques of mechanical characterization of dental composites were static, such as nanoindentation or three-point bending test, in recent years dynamic mechanical analysis (DMA) is becoming increasingly used [**15-18**]. Among the advantages of this technique for determination of elastic modulus is its low invasiveness for the specimens, the more complete picture provided about the viscoelastic behavior intrinsic in the composite matrix, and the capability to better correlate with the chemical effects (regarding composition and structure), for example as for assessment of curing extent and glass transition temperature [**16**].

We investigated the viscoelastic properties of our composites by DMA. Fourier transformed infrared spectroscopy (FTIR) was carried out to determine the degree of conversion (DC). The size and distribution of the fillers in the solid samples was characterized by atomic force microscopy (AFM) performed on polished specimens, which allowed to access an inner section of the composites, which was compared to the expected loading. AFM also allowed performing nanoindentation, whose results were compared to those of DMA.

Experimental

Materials and methods

Resin matrix: Bisphenol-A-glycidyldimethacrylate (BisGMA) was first sonicated for 15 min to decrease its viscosity. Then triethylene glycol dimethacrylate (TEGDMA) was added (30:70 wt), as a viscosity decreasing co-monomer, and the mixture was spatulated for 3 min. Finally the photo-polymerization system of camphorquinone (CQ) and dimethyl amino ethyl methacrylate (DMAEMA) was added (1:1 wt, total 0.5%wt to the co-monomer), followed by 3 min more spatulation. All organic products were supplied by Sigma-Aldrich (Milan, Italy).

In case of filler loading, the respective particles were added in 10 or 50% wt proportion of the overall organic matrix paste, and the system was spatulated again for up to additional 15 min for the highest loading cases. The paste was then sonicated for 15 min and finally poured into a clean mold of glass, and placed in a bell rest chamber pumped to low vacuum (~100 mbar) to remove air bubbles formed during spatulation.

Filler materials

We selected two commercial alumina powders, namely 'powder' 265497 (Sigma-Aldrich, mean particle size >10 µm), called micro-alumina in the following, and 'nano-powder' 13-2610 (Strem Chemicals, exact size unknown), called nano-alumina in the following. A third type of composite fillers considered for comparison (positive-control sample) was based on ball-milled glass. The respective results come from a previous experiment, in which the average glass particle size was close to 1 µm [**19**].

The apparent particle size of the nano-alumina filler was measured by dynamic light scattering (DLS) in isopropanol (IPA) suspensions, loaded in a polystyrene cuvette and analyzed in a Nano-ZS setup (Malvern Instruments, UK). In order to obtain the least amount of particle aggregation and measure a size as close as possible to individual primary particles, the suspensions were progressively diluted to a factor (1/3)x at each consecutive step, starting from a concentrated IPA suspension (~5 g/L) and going on until the measurement provided sufficient optical density required for statistical analysis. After each diluting step the cuvette was sonicated for 3 minutes and then moved as fast as possible (~10 s scale) to the measurement, which was carried out without dead pause times. The final measurement provided a mean nano-alumina particle size of ~60 nm.

We assume that all particles were suspended and no precipitate developed. However, the DLS particle size in liquid is probably quite different from that occurring in the cured resin at the solid state. Therefore, a much more accurate evaluation was carried out after curing and polishing the samples, by means of AFM (see Section 3.2 Composites morphology).

Photo-curing procedure and evaluation

The mold used for shaping the solid specimens was made of glass slides for optical microscopy (~1 mm thickness). These slides were assembled together on the main plane by gluing them with cyanoacrylate on three sides and one short notch as the fourth side, facilitating specimen removal after polishing. For the larger plates closing the opposite sidefaces on top and bottom of that plane, one was glued and the other was kept in place by metallic clamps. Glass was used to allow for photo-polymerization on two opposite large sidefaces, to avoid non-uniform in-depth curing. Irradiation was carried out (5 min per side) with an X-Cite 120 lamp (EXFO, Canada), band-pass filtered (Semrock filter, USA) at a 455-490 nm wavelength.

In order to verify the conversion of the co-monomer paste into a polymerized resin, Fourier transformed infrared spectroscopy (FTIR) was carried out for all the specimens at room temperature (RT) in ambient air, both soon after mixing on a small paste droplet, and after specimen bars irradiation. The FTIR spectra were acquired by a Vertex 70 spectrometer (Bruker, USA) in attenuated total reflection configuration, with a spectral resolution of

4 cm^{-1}. Each spectrum was the average of 50 scans, and was apodized by applying the Blackman-Harris 3-term correction function. The spectra were baseline-corrected by third order polynomial and normalized thereafter.

DMA

All the materials were shaped with the glass mold to be rectangular beams of 13 × 35 × 2 mm^3 in size. On these samples we performed DMA by means of a Q800 setup (TA Instruments, USA), with instrument compliance of less than 0.2 µm/N, as determined by a prior calibration in static loading mode. We carried out DMA measurements in single-cantilever mode, under strain control in the materials linear regime, (maximum applied strain of ±35 µm). Temperature sweeps at strain frequency of 0.1, 1 and 10 Hz were carried out in a range of +2 to +62°C (with 5°C steps, 5°C/min rate), since this should represent well the limit values occurring in human mouth in normal operating conditions, when ingesting from hot food to icy drinks. For reaching the lowest temperatures in this range, liquid nitrogen was used as a coolant. During the temperature scans both the in-phase (real) and the out-of-phase (imaginary) parts of the complex modulus were measured, namely storage modulus E' and loss modulus E", respectively.

AFM imaging and nanoindentation

We used a MFP-3D AFM (Asylum Research, USA). AFM imaging was carried out in tapping mode with gold coated silicon probes NSG20 (NT-MDT, Russia), consisting of a cantilever with nominal spring constant and resonance frequency of ~60 N/m and ~450 kHz, respectively, and of a terminal transverse pyramidal tip with apex diameter and full aperture angle of ~20 nm and ~22°, respectively. For both imaging and nanoindentation, the same specimens already measured previously in DMA were used. A small area (~2 mm diameter) of the specimens was first polished , in order to expose their inner compositions under the top surface. To this goal we used a 656 Dimple Grinder (Gatan USA), working for 1 hr with a felt ring loaded with 0.25 µm diameter diamond particles. It was estimated that at least the top 100 nm are removed under the described treatment. Before AFM the surfaces were wiped clean with ethanol-wet lens paper.

AFM nanoindentation was carried out by means of AFM 'force spectroscopy' mode, collecting force-distance curves on square arrays of specimen sites. The AFM probe was calibrated in air for determination of the cantilever spring constant. Since in previous similar measurements on different materials [**19**] we observed little adhesion effects due to ambient air moisture on the indentation region of the curves (typically above 25% of the maximum indentation force), we worked in air also for nanoindentation. The curves had z actuation loops of 1 µm range and 1 Hz frequency. After acquisition, the indentation δ was calculated from the actuator movement Δz and from the change in cantilever deflection ΔD (partially compensating the former) as δ=Δz-ΔD. The force-indentation data were finally fit to the Hertz model of elastic contact, using the loading part of the force loop, to find the elastic modulus values AFM. Different from a previous work on different composites [**19**], here we fitted the curves with a sphere as the tip shape. In fact, the used tips were previously blunt on purpose by scratching them onto silicon, and resulted in a rounded apex of ~250 nm radius of curvature, as determined by scanning electron microscopy performed before and after AFM (images not shown). At the considered scan sizes (50 µm with 256^2 pixels, i.e. ~200 nm/pixel) these blunt tips did not involve any reduction in lateral resolution even for the finer topographical imaging, which was carried out before the rougher nanoindentation mapping scan (20 µm with 40^2 pixels, i.e. 500 nm/pixel). On the other hand, the blunt tips made the uncertainty on the Hertz fitting model less dramatic as with sharp tips [**20**].

Results and discussion

Resin curing evaluation

The emitted power of our blue light was ~60 mW. Glass from the mold face should reflect off ~8% of incident light. Even if 100% absorption of the dose reaching the specimens is assumed, when our lamp power is compared to commercial LED (~1000 mW), a simple exposure reciprocity law between incident irradiance p_{inc} and exposure time t, p_{inct}=constant, should result into 210 min total exposure time [**19**]. However, it was observed that sonicating the paste before pouring it into the mold resulted in effective curing, with times as short as mentioned above (10 min total). The real effectiveness of this exposure recipe has been evaluated by means of FTIR.

Table 1. DC for the different samples compared in the present study, at the two different levels of weight loading considered, Φw = 10 and 50%.

Type of filler	Φ_w (%)	DC (%)
Nano-alumina	10	63
	50	62
Micro-alumina	10	64
	50	70
Glass	10	59
	50	69
None (bare resin)	0	57

Spectroscopic analysis of polymerization was carried out on the specimens before any mechanical measurements by DMA and AFM. From the FTIR spectra, a change in the bands centered around 1637 and 1580 cm^{-1} was observed, with a relative increase of the second one, corresponding to the stretching of the aliphatic and aromatic (i.e. ring) C=C bonds, respectively. After this effect, we evaluated the degree of conversion (DC) of the

monomer mixture into the polymer, by comparing the above peak intensities according to DC=100[1-(I_{1637}/I_{1580})polymer/(I_{1637}/I_{1580})paste], with obvious meaning of the subscripts. The results are reported in **Table 1**.

The spectra used for DC evaluation were all measured one day after curing and no aging was evaluated at later times, involving post-curing and possible absorbance of ambient moisture. From Table 1 it can be seen that overall the DC was mostly in the 60-70% range, which can be considered a good level, representing complete curing in all cases. The peculiar exposure on both opposite sides of the specimens through the glass walls has probably facilitated the photo-polymerization. With respect to previous work [**19**], despite the different exposure time (total 10 min with preliminary sonication instead of 210 min without sonication) the DC of bare resin was very well reproduced (59% instead of ~57%), confirming the validity of the chosen curing recipe and the strong effect of more uniform mixing of paste after sonication. Probably sonication is effectively mixing the resin components, providing the finest combination of co-monomer and light curing system molecules, enhancing the polymerization reaction efficiency.

The DC of alumina composites is even higher than that of the bare resin. In the case of this filler material, obviously the effect of reflecting light off the specimen (decreasing the irradiation efficiency) is overwhelmed by the internal reflection and absorption (which on the contrary facilitates the curing, together with the reduced resin volume due to filler loading).

On increasing the loading from Φ_w=10 to 50%, whereas the DC increased consistently for glass, it did not substantially increase neither for micro-alumina nor for nano-alumina. We will see later on that, concurrently, the elastic (storage) modulus of glass at 1 Hz and body temperature (BT, 37°C) did not increase significantly, whereas for micro-alumina it roughly doubled, and for nano-alumina it underwent a five-fold increase. Obviously, even for the same resin system, evaluation of the composite mechanical properties according to the DC can be questionable when different filler materials are used.

In this experiment, at the higher loading level (50%wt) also the nano-scale alumina was successfully mixed with the resin, different from the nanosilica of [**19**]; additionally, both the micro- and nano-alumina were properly cured, different from the titania of [**19**]. This was due to the nano-alumina probably not showing such a huge specific surface area as the nanosilica (~200 m^2/g [**19**]), so being properly void of large amount of trapped air, and capable of being mixed even without bonding agent on its surface or plasticizing solvents. For the good curing, while still being white reflecting such as titania, alumina is obviously not as an effective white pigment as the latter material, which is used in this respect in several fields, from painting to sunscreen.

Composite morphology

The nominal micro-alumina particle (>10 μm) should make of the respective composite an old-fashioned macro-filled. The nano-alumina particles (10-100 nm order) would rather form a micro-filled composite, instead. In fact, since in neither case a monodisperse particle size distribution is foreseen hybrid composites are expected, i.e. nano-hybrid and micro-hybrid for nano-alumina and micro-alumina, respectively, according to recent classifications [**3**]. To find out the actual size and distribution of fillers (or their aggregates) in the solid samples, the polished specimens were imaged with AFM in air in tapping mode. Representative images are shown in **Fig. 1**. A higher uniformity of the fine-grained nano-alumina is observed in **Fig.1a** as compared to micro-alumina in **Fig.1b**, whereas the glass composite **Fig.1c** is somewhat intermediate, according to the respective filler particle size.

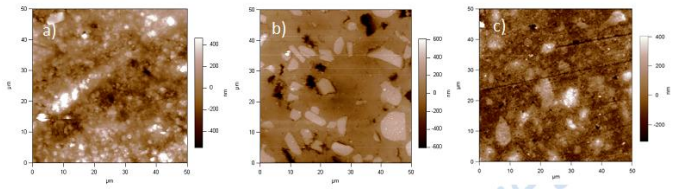

Fig. 1. Typical images of composites with loading Φw=50% for the different fillers: a) nano-alumina, b) micro-alumina, c) glass.

From the AFM images the size, shape, and relative area occupied by the fillers (coverage f) can be evaluated. The latter quantity, in particular, can be compared to the volume loading Φ_v, after appropriate conversion of the mass loading Φw. As a result, an overall good agreement of f with Φv appears in **Table 2**, when the dark areas of the removed fillers (coverage fwear) are also considered in the images, (such that $\Phi v \cong f + f_{wear}$). In the nano-alumina composite **Fig. 1a**, as well as partly in the glass one **Fig.1c**, most depressions (dark zones) were not considered as being associated with fwear, but rather due to normal roughness of the surface, resulting from the more fine-grained filler in combination with the polishing.

Table 2. Coverage of filler particles f and of apparently removed filler particles f_{wear}(associated with the dark pits), and the respective volume loading Φv, for the various composites considered.

Type of filler	Φ_w (%)	Φ_v (%)	f (%)	f_{wear} (%)
Nano-alumina	10	~3	2.9	0.1
	50	22	20	1
Micro-alumina	10	~3	2.5	0.3
	50	22	18	5
Glass	10	~5	4.8	0.5
	50	31	26	2

Sample mechanical properties

The DMA thermal scans at 1 Hz (roughly the mastication frequency) are shown in **Fig. 2**. In particular, **Fig. 2a**) reports the storage modulus E', while in **Fig. 2b**) we

decided to report the loss ratio (or damping factor) tanδ=E''/E'. This is at the same time proportional to the loss modulus E'' and shows the relative weight of this component of the total modulus (E= $\sqrt{(E'^2+E''^2)}$~E'), stressing the importance of the viscous flow behavior of the material.

In **Fig.2a**, the flexural elastic modulus E' is for all the composites higher than for the bare resin (~0.8 GPa at BT), as expected. On increasing the loading, the two types of alumina composites showed both a significant increase in modulus, wheras this was not the case for glass (from ~1.9 to ~2.2 GPa only, at BT). For micro-alumina the modulus approximately doubled (reaching ~2.3 GPa at BT), whereas for nano-alumina it underwent a fivefold increase, reaching ~6.8 GPa at BT. This value is almost in the range of commercial materials (usually around 10 GPa), without occurrence of filler silanization.

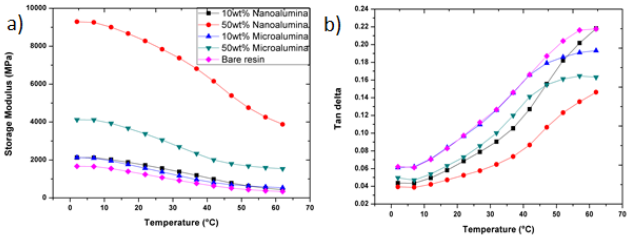

Fig. 2. DMA results showing storage modulus E' and loss ratio tanδ=E''/E' for all composites as well as the bare resin, (legend see figure inset).

On increasing the temperature, E' decreases for all composites, due to the increased molecular mobility of the polymer chains. The decrease is smooth and no glass transition appears, as shown by the absence of clear peaks in **Fig. 2b**. The nano- and micro-alumina composites with Φ_w=10% show no significant difference between them in both E' and tanδ, along with only a minor average increment with respect to the bare resin. In fact, the total modulus E (not shown) is quite constant. These effects are an evidence of too low loading for the current application. On the contrary, for Φ_w=50% a difference appears between nano- and micro-alumina. When considering the values at BT, whereas both alumina composites with Φ_w=50% show higher E' than the Φ_w=10% ones (~0.96 GPa), the nano-alumina composite is much stiffer than the micro-alumina one (~6.8 GPa vs 2.3 GPa). Probably, for Φ_w=50% the smaller filler provides a better dispersion and thus a higher uniformity of the inorganic phase, as shown in **Fig. 1a**, so improving its reinforcement effect.

From **Fig. 2b** it is clear that all the composites show less damping as compared to the bare resin, because some strain is made via the stiff fillers, resulting in less energy dissipation. On increasing the loading, tanδ becomes lower at all temperatures for both alumina fillers, as the fillers obviously cause some inhibition of the chain segments relaxation.

The effect of the dynamic strain frequency has been described in **Fig. 3**. There, both storage modulus E' (**Fig. 3a)** and loss ratio tanδ at BT (**Fig. 3b)** have been plot. It can be seen that E' increases with f for all the materials. The highest relative increase is for the bare resin (+28% and +57% at 1 Hz and 10 Hz with respect to 0.1 Hz values, respectively). The second highest increase occurs for the micro-alumina samples (+26% and +53% and +19% and +39% for the Φw=10 and 50% samples, respectively). In fact, the glass composites, which both have values in the same range as micro-alumina with Φ_w=50%, show increases of +10% and +22% and +12% and +23% for Φw=10 and 50%, respectively. The nano-alumina samples show lower relative increases (+16%, +33% and +10%, +19% for Φ_w=10 and 50%). However, yet with the lowest increase rate, the values for nano-alumina with Φw=50% are at all frequencies much higher than for all the other materials (about three times as much the micro-alumina and the glass with Φ_w=50%).

Additionally, the loss ratio values tanδ (**Fig. 2b**) monotonously decrease for all samples but for micro-alumina with Φ_w=10% and for both the glass samples (where it stays constant in particular for Φ_w=10%). This means that the behavior of these composites becomes less viscous and more elastic at higher frequencies, as expected.

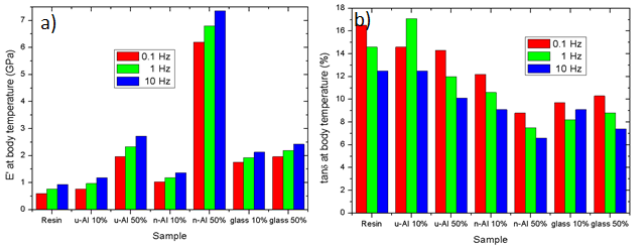

Fig. 3. Modification of a) storage modulus E' and b) loss ratio tanδ, when changing strain frequency between 0.1, 1 and 10 Hz, at BT, for the different composites.

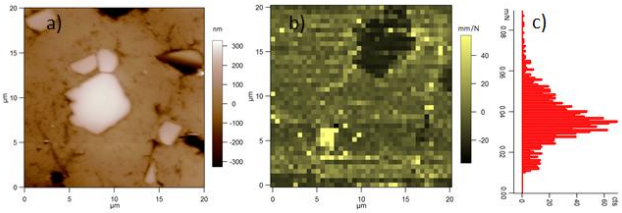

Fig. 4. Example of AFM nanoindentation result: a) topographic image, b) map of compliance, c) histogram of compliance values appearing in b).

To complement the dynamic viscoelastic characterization by DMA, we carried out also static elastic characterization of our composites by AFM nanoindentation. One of these measurements is shown in **Fig. 4**, where the 256^2 pixels topography (**Fig. 4a**) and the subsequent 40^2 compliance map (inverse of the force-indentation curve slope, **Fig. 4b** in the same area of a micro-alumina sample with Φ_w=50% are shown, as an example. The smaller area used here in AFM nanoindentation (scan size 20 μm with respect to the 50 μm of **Fig. 1** allows one to identify clearly individual fillers also in the rough spatial mapping of nanoindentation (40^2 pixels in **Fig. 4b**, despite the relatively high thermal drift of the imaged area towards the upper-right direction (~10 μm/hr) appearing in the latter image. In **Fig. 4c**, the histogram of compliance levels distribution spanned in the

color scale of **Fig. 4b** is also shown. Clearly, both the intermediate level of the resin (most data points) and the small peak at lowest compliance (the stiff alumina filler, dark area in **Fig. 4b** appear in the histogram. The void in the resin surface (bottom left of the image), appearing instead as a small region of very high compliance in **Fig. 4b**, has too few pixels to give rise to a peak in the histogram, and only results in few sparse datapoints on the high compliance tail of the distribution.

Each pixel in **Fig. 4b** comes from a different individual force-indentation curve. These curves on each AFM map have been analyzed and fit to the Hertz model independently, and their population has been used to find an error on the respective value of elastic modulus E_{AFM} thus obtained, takes as ±1 standard deviation of the measurements.

Whereas BT can be considered the most important temperature of reference for the properties of the considered materials, since this is the operating temperature for the future clinical applications, for a better comparison with AFM nanoindentation measurements, which are carried out in air without temperature control, the DMA values of storage modulus at RT have been extracted from **Fig. 2**, termed E_{DMA}, and are plotted together with EAFM in **Fig. 5**.

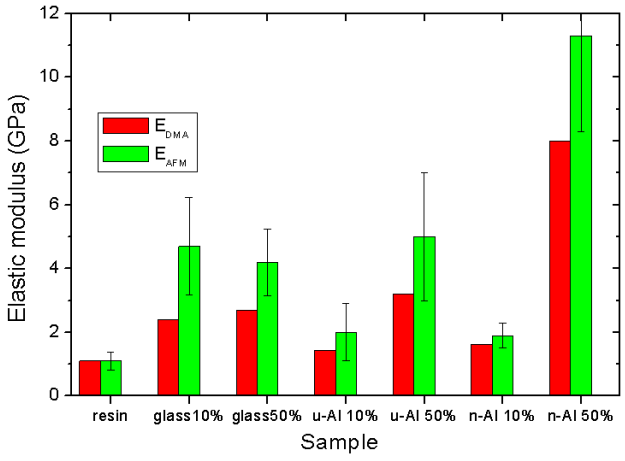

Fig. 5. Comparison between values of elastic modulus (storage modulus E') obtained from DMA at 1 Hz (E_{DMA}) and from AFM static nanoindentation(E_{AFM}), at RT, for the different materials.

It can be seen that in all cases $E_{AFM}>E_{DMA}$, except for the bare resin sample, which was set on purpose to the same value in both cases, in order to fix some parameters of the Hertz fit (namely the contact point offset in the force-indentation curves [**19**]). In fact, it is known that the flexural modulus should rather be higher than the compressive one, in dental restorative composites [**21, 22**]. However, as our composites do not have bonding agent, they are more likely effective in reinforcing the resin in bare compressive mode than in mixed flexural mode, which is comprised of a compressive and tensile strain simultaneously present at each instant on the opposite sides of the specimen beams. In a previous experiment [**19**], the excess of E_{AFM} was approximately +100% as compared to E_{DMA}, whereas here the increase is more limited, roughly +50%. The large round tip model may have played a role, making the present deviation smaller.

In any case, the ranking in E_{AFM} is the same as that in E_{DMA}, showing both nano- and micro- alumina composites be lower in modulus than the glass ones, the micro-alumina with Φw=50% being the same level, and the nano-alumina with Φw=50% performing much better. The latter in particular is at RT as high as ~8.0 GPa according to DMA and 11.3±3 GPa according to AFM, which is as high as some commercial composites with complex bonding agent treatment and much higher filler loading obtained with lower stiffness fillers.

Conclusion

Obtaining a high enough elastic modulus, not much lower than that of dentine (~18 GPa), is still one of the most important goals in newly developed dental restorative composites. Values around ~10 GPa are usually reached with relatively low stiffness fillers (glass, typically ~70 GPa) bonded to the resin with silane coatings. In addition to the importance of appropriate filler-matrix bonding, we show here that by using stiffer filler materials (alumina >300 GPa), a relatively high modulus can be reached in composites (8-11 GPa) even with comparatively low loading (Φ_V=22%) and without chemical filler coating. Whereas compressive stress due to mastication is obvious in dental restorative materials, flexural stress is also important, especially in crowns and extensive restorations. Therefore, for our alumina composites we measured both compressive and flexural modulus, by AFM nanoindentation and DMA, respectively. AFM nanoindentation gives compressive modulus that ranks similarly to flexural (storage) modulus from DMA, but is ~50% higher. At the considered loading, for the same alumina filler material, nano-particles provide better uniformity as well as highest modulus, despite formation of aggregates and absence of bonding agent. Therefore, use of ultra-stiff filler materials such as alumina (and possibly zirconia and diamond), especially in nanoscale size, appears a viable strategy to improving the elastic properties of dental composites.

Reference

1. Moszner N., Salz U., Program of Polymer Science 2001; 26:535-576.
2. Chen M.-H., J Dent Res 2010; 89:549-560.
3. Ferracane J. L., Dental Materials 2011; 27:29–38.
4. Uskoković V., Bertassoni L.E., Materials 2010; 3:1674-1691.
5. Sharma S., Cross S. E., Hsueh C., Wali R. P., Stieg A. Z., Gimzewski J. K., Int J MolSci 2010; 11:2523-2545.
6. Wahl M. J., Quintessence Int 2001; 32:525-35.
7. Deliberation of the European Council, May 27th, 2011; URL: http://www.assembly.coe.int/Mainf.asp?link=/Documents/WorkingDocs/Doc11/EDOC12613.htm
8. Bayne S. C., Thompson J. Y., Swift Jr E. J., Stamatiades P., Wilkerson M., J Am Dent Assoc 1998; 129:567-77.
9. Salerno M., Derchi G., Thorat S., Ceseracciu L., Ruffilli R., Barone A., Dent Mater 2011; 27:1221–1228.
10. Salerno M., Patra N., Diaspro A., Dental Materials, in press, 10.1016/j.dental.2011.10.007.
11. Salerno M., Patra N., Derchi G., Diaspro A., Science of Advanced Materials, in press.
12. Shinzato S., Kobayashi M., Choju K., Kokubo T., Nakamura T., Journal of Biomedical Materials Research 1999, 46;287-300.

13. Kobayashi M., Shinzato S., Kawanabe K., Neo M., Matsushita M., Kokubo T., Kikutani T., Nakamura T., Journal of Biomedical Materials Research 2000; 49:319-327.
14. Wang Y., High elastic modulus nanopowder reinforced resin composites for dental applications, PhD thesis 2007, University of Maryland.
15. Vidal-Mesquita R., Dynamic mechanical analysis of direct and indirect dental composite resins, PhD thesis 2006, University of Tübingen.
16. Jacobsen P. H., Darr A. H., J Oral Rehabil 1997; 24:265-273.
17. Yang J. M., Li H. M., Yang M. C., Shih C. H., J Biomed Mater Res 1999; 48:52-60.
18. Ryou H., Niu L.-N., Dai L., Pucci C. R., Arola A. A., Pashley D. H., Tay F. R., J Dent Res 2011; 90:1122-1128.
19. Thorat S., Patra N., Ruffilli R., Diaspro A. Salerno M., Dental Materials Journal, accepted.
20. Salerno M., Measurement, in press.
21. Darvell B. W., editor, Materials science for dentistry, 9th ed. Sawston, Cambridge: Woodhead Publishing Limited, 2011.
22. Braem M., Davidson C. L., Vanherle G., Van Doren V., Lambrechts P., J Dent Res 1986; 66:1036-1039.

